J Therm Anal Calorim (2011) 103:835–843
DOI 10.1007/s10973-010-1129-6

Thermal study of sandstones from different Czech localities

E. Plevová · L. Vaculíková · A. Kožušníková · T. Daněk · M. Pleva · M. Ritz · G. Simha Martynková

Received: 5 August 2010 / Accepted: 25 October 2010 / Published online: 12 December 2010

Abstract Thermal analysis is a useful tool for determination of the rock's thermal behavior. The thermal behavior of the rock is affected by both its composition and structure. This study presents the application of thermogravimetric, differential thermal, and thermomechanical analyses for the characterization of the selected Czech sandstone samples. The detailed study of mineralogical composition was carried out by FTIR spectroscopy, X-ray diffraction, and optical microscopy. Thermal expansion during heating up to 1,000 °C, together with the coefficient of thermal expansion showed almost the same values for all the studied sandstone samples. Nevertheless, the residual thermal expansion varied depending mainly on the composition. In the case of higher content of quartz, the thermal expansion showed higher values. With increase of carbonate, glauconite, or clay mineral volume, the residual thermal expansion decreased. Factors such as grain size or shape of particles did not significantly influence the observed thermal expansion values.

Keywords Thermomechanical and differential thermal analysis · Optical microscopy · Sandstones

E. Plevová (✉) · L. Vaculíková · A. Kožušníková
Institute of Geonics AS CR, Studentská 1768,
708 00 Ostrava, Czech Republic
e-mail: eva.plevova@ugn.cas.cz

T. Daněk · M. Ritz · G. Simha Martynková
Technical University of Ostrava, 17. listopadu 15,
708 33 Ostrava, Czech Republic

M. Pleva
Elvac, Hasičská 53, 700 30 Ostrava, Czech Republic

Introduction

Sandstone is a sedimentary rock formed from sand-sized grains. The spaces between grains may be filled with cement of silica, carbonate, or clays. The principal mineral constituents of the grain framework are quartz, feldspar, and rock fragments. Sandstones are quarried for use mainly as building stone. Sandstone has represented the traditional stone-cutting material, being used in the Czech republic for a long time. The usage of green Cenomanian sandstone from Eastern Bohemia (Rychnov nad Kneznou districts) has been known since the thirteenth century as a building material of local castles (Potstejn, Zampach), palaces, religious buildings, as well as significant local sculptural material. In the nineteenth century, green sandstone played an important role in the construction of railway lines (Hradec Kralove–Lichkov) and river bridges. Next well-known medium-grained sandstone from northern edge of the Beskydy Mountains (Reka quarry) and light quartz sandstone from area near Horice town are traditionally used for exterior cladding, garden architecture, as well as outdoor designs [1, 2]. Because of their abundance, diversity, and mineralogy, sandstones are important to geologists, e.g., as indicators of erosional and depositional processes etc. [3–6].

The effect of temperature on the resultant sandstone properties seems to be a difficult problem significantly effected by composition and structure. Temperature increase causes the phase and polymorphic sandstone transformation connected to thermal expansion with following appearance of tensions and cracks in minerals and rock structure. After consequential temperature decrease, developed tensions and cracks still influence the process. Also the differences in mineralogical composition cause different thermal behaviors of sandstone as the consequence of various chemical reactions (dehydration, dehydroxilation, dissociation, etc.)

and phase or polymorfic transformations [7, 8], as well as the different mechanical properties [9–13].

In this article, a detailed study of eight Czech sandstone samples based on investigations carried out using thermogravimetry, differential thermal analysis and thermomechanical analysis along with optical microscopy, X-ray powder diffraction, and FTIR spectroscopy is reported. The detailed study has included mainly the effects of sandstone composition and structure on residual thermal expansion and the effect of phase transformation process during the heat stress of material.

Samples

For this investigation, eight Czech different sandstone samples were chosen for the characterization of their thermal behavior particularly with regard to thermal expansion. Samples of glauconitic sandstone from Zamel quarry (7643), white sandstone from the same quarry (7642), medium-grained sandstone from Reka quarry (10197), sandstone from Doubrava mine (8959), sandstone from Cerveny Kostelec quarry (10577), and three sandstones from Darkov mine (10167, 10168, and 10169) were used for this study. These samples were chosen not only because of their different medium grain sizes, sortings, or shapes of grains but also because of their different stratigraphies. The schematic map of Czech republic including the quarry localities of the studied samples is shown in Fig. 1.

Methods

Optical microscopy

Thin sections were prepared from all the test samples and were oriented in the directions A, B, and C of specimen. The orientation was arranged in three directions perpendicular to each other (coordinate system ABC). Prepared thin sections were observed under BX 50 OLYMPUS polarization microscope with a DVC camera connected to a PC. The photomicrographs were taken by a microscope model: NICON ECLIPSE 80i. The analysis was performed in polarized light at 20 times magnification. Size and possible preferred morphological orientation of grains were determined for every thin section (coordinate system ABC).

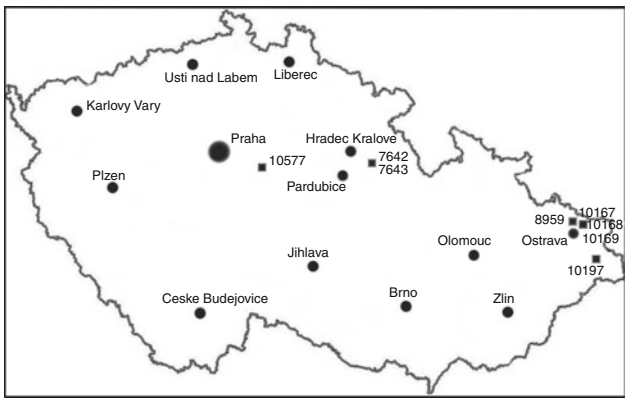

Fig. 1 The schematic map of Czech republic including the quarry localities

X-ray diffraction and FTIR spectroscopy

X-ray diffraction (XRD) was performed using Bruker D8 Advance X-ray powder diffractometer. XRD patterns were obtained using position-sensitive Vantec detector, CoK_{α} radiation, and operating parameters of 35 kV, 25 mA, 0.03° 2θ increment, and time at step 1 s.

Infrared spectra were recorded using Nicolet Avatar 320 FTIR spectrometer equipped with a DTGS/KBr detector. The KBr pressed-disk technique (2 mg of sample and 200 mg of KBr) was used. The spectra were measured by accumulating 64 scans at 4 cm^{-1} resolution in the spectral range from 4,000 to 400 cm^{-1}.

Simultaneous thermogravimetry and differential thermal analysis

Thermal properties were investigated by simultaneous thermogravimetry and differential thermal analysis using the thermal analyzer, Setsys 12 Setaram equipped with thermal measurement head, TG ATD Rod. The TG/DTA curves were recorded in a static air atmosphere with a heating rate 10 °C min^{-1} to the final temperature 1,000 °C. The sample mass used was about 50 mg.

Thermomechanical analysis

Thermal expansion was determined by thermomechanical analysis using the thermal analyzer, Setsys 12 Setaram equipped with thermal measurement head TMA quartz. Test specimens (cube 10 × 10 × 10 mm) were heated in a furnace and transmitted by means of spherical-ended QUARTZ probe with a 5-mm diameter. Measurement of deformation was performed by compression with a probe resting on the sample and the load adjusted to nil value. Sample cubes were prepared according to the three principal axes of the reference coordinate system ABC mentioned above.

Resultant TMA curves show the measurement of a specimen′s dimension (length) as a function of temperature under constant compressive load and following conditions : final temperature 1,000 °C, and heating rate 20 °C min^{-1}.

This technique was used to determine residual thermal expansion (ε), thermal expansion obtained during heating (ε_H), and the coefficient of thermal expansion (α_H) in the temperature interval 25–1,000 °C.

Results and discussion

Optical microscopy

Grain size, sorting, shape of grains, type of contact among the grains, and characteristic of rock structure were determined by optical microscopy (Table 1). The porous structure was determined for the most of tested samples except for two samples. For the samples, 10577 and 11167, the basal structure was determined. The shape of clasts and grains varied from angular to rounded with most of them being subangular. Sorting of samples varied from good to poor: the samples, 7643 and 11167, were of good sorting: and the samples, 10555, 10577, and 11168, were of poor sorting. Medium grain size ranged from 0.17 mm (sample 7642) to 0.68 mm (sample 11169). The contacts among the grains and clasts were found in limited areas; only two samples (10577 and 11167) showed the grains being spread out in matrix.

The petrographic analysis did not reveal many differences in the quality of the sample. Major phase was the quartz for all the analyzed samples followed by constituents like rock fragments, feldspar, muscovite, biotite, and carbonate. Carbonate was found as separate or as a part of binder in the samples 8959, 10197, 10577, 11167, and 11168. Only the sample 7643 contained relatively a large amount of glauconite (over 20%). For illustration, the photomicrographs of the samples: 7642 (with the smallest medium grain size), 10577 (with the middle medium grain size), and 11169 (with the highest medium grain size) are shown in Figs. 2, 3, and 4.

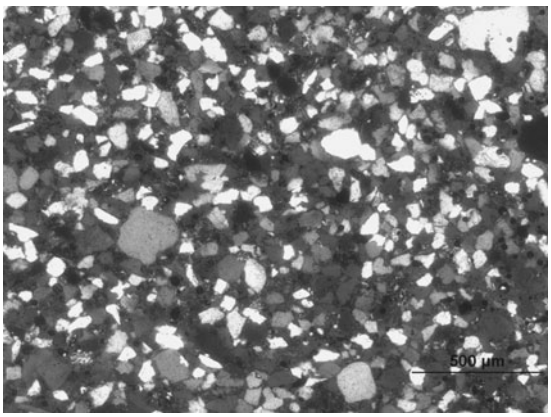

Fig. 2 Photomicrographs of the sandstone microstructure—thin section no. 7642—Zamel quarry (transmitted light, crossed polarizers)

XRD and FTIR measurements

X-ray diffraction analysis was used to evaluate patterns considering the phase analysis. Major phase was quartz for all the analyzed samples. Illite was also found in all the tested samples. The carbonate was identified as calcite (in samples 10197 and 11168), dolomite (in samples 10577 and 8959), and siderite (in sample 10167). Also the presence of chlorite (samples 7642, 7643, 11167, 11168, and 11169), kaolinite (sample 7642), muscovite (samples 8959, and 11169), mica (samples 8959, 10197, 10577, and 11167), glauconite (7643) and feldspare (samples 8959, 10197, 10577) was observed. The presence of individual phases was evaluated by software ICCD 2004 (EVA) with an extensive database of minerals and other inorganic substances. The measured XRD patterns and results were also compared with the previously published data [14–16]. For illustrative purposes, XRD patterns are given in Figs. 5, 6, 7, and 8. In XRD patterns, muscovite is signed as M, mica (biotite/phlogopite) is signed as Mc. and the other components are fully marked.

Table 1 Localization and microscopic characterization of tested samples

Sample	Localization; stratigraphy	Medium grain size M_d/mm	Sorting	Shape of grains	Structure	Character of grain contact
7642	Zamel; Cretaceous	0.17	Medium to poor	Subrounded	Porous	In limited areas
7643	Zamel; Cretaceous	0.23	Good	Subangular	Porous	In limited areas
8959	Mine Doubrava; Carboniferous	0.59	Medium to poor	Subangular	Porous	In limited areas
10197	Reka; Cretaceous	0.28	Medium to poor	Angular	Porous	In limited areas
10577	Cerveny Kostelec; Permian	0.37	Poor	Rounded	Porous to basal	In limited areas; some places without contact
11167	Mine Darkov; Carboniferous	0.22	Good	Subangular	Porous to basal	In limited areas; some places without contact
11168	Mine Darkov; Carboniferous	0.56	Poor	Subangular	Porous	In limited areas
11169	Mine Darkov; Carboniferous	0.68	Medium	Subangular	Porous	In limited areas

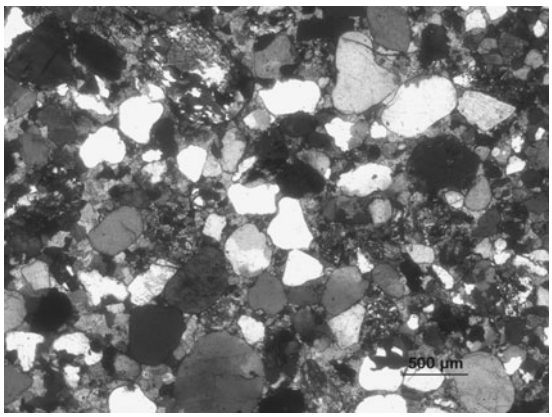

Fig. 3 Photomicrographs of the sandstone microstructure—thin section no. 10577—Cerveny Kostelec quarry (transmitted light, crossed polarizers)

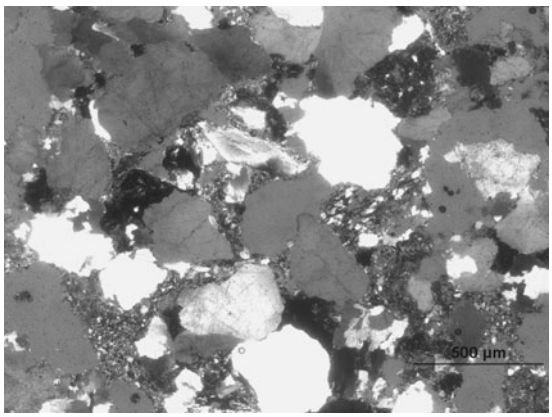

Fig. 4 Photomicrographs of the sandstone microstructure—thin section no. 11169—Doubrava mine (transmitted light, crossed polarizers)

Method of infrared spectroscopy with Fourier transformation was used to complete the results of the mineralogical composition. The major component was the quartz for all the tested samples (bands approx. at 1180, 1124, and 1081, characteristic doublets 795 and 778 cm^{-1}). Illite/muscovite (bands approx. at 3440, 1030, and 1021 cm^{-1}) was also found in all the tested samples. These were followed by other compounds like chlorite (bands approx. at 1635, 1087, 985, 650 cm^{-1}) found in samples 7642, 7643, 10555, and 10168; mica (bands approx. at 3628, 1625, 1063 cm^{-1}) found in samples 7643, 10577, 11167, and 11169; kaolinite (bands approx. at 3694, 3668, 3645, 3619, 1008, 938, and 913 cm^{-1}) found in sample 7642; and feldspar (with its characteristic sharp low-intensity bands at the interval range of 800–400 cm^{-1}) found in samples 8959, 10197, 10577, 11169, and 11169. The presence of carbonate (bands approx. at 1420, 878, and 712 cm^{-1}) was confirmed in samples 8959, 10197, 10577, 11167, and 11168. The measured spectra were compared with the records of the published data [17–19]. The results from FTIR correspond well with those from XRD measurement; a few differences are probably caused by the quite low volume of some components, or/and the presence of mixed structures of clay minerals. The problems associated with the identification of mixed structures of clay minerals using infrared spectroscopy have been pointed out by several authors [20–22]. For illustrative purposes, FTIR spectra of sandstone samples are given in Figs. 9, 10, and 11.

TG and DTA measurements

Thermal behaviors and mineralogical compositions of the studied samples were determined using simultaneous thermogravimetry and differential thermal analysis. Quartz was found in all the tested samples. The presence of carbonate (calcite, dolomite, or siderite) was detected in five samples, which corresponded well with the results of X-ray diffraction. Associated minerals determined by XRD and FTIR methods could not be confirmed by simultaneous TG/DTA because of their really small amounts or overlapping effects (corresponding with releasing of constitution water, crystal lattice breaks, or recrystallization) with carbonate dissociation effect (700–1,000 °C) or endotherm effect due to polymorphic transformation of quartz, which is undergoing α–β modification at 573 °C [23, 24]. Only the presence of minerals such as kaolinite, illite, chlorite, and glauconite could be confirmed by small weight loss at temperature intervals belonging to the dehydroxilation of these minerals, approximately at the temperature interval of 300–600 °C [25]. Their thermal effects on DTA curves were overlapped and impacted by endotherm connected to modification of the relatively the large amount of quartz [26]. TGA was used to determine carbonate content in the tested samples, it was an average determination of five measurements. This determination could be made because of the absence of other thermal effects connected to mass loss in the temperature range of 700–1,000° C. Dissociations of calcite and siderite take place in only one stage, while that of dolomite takes place in two stages (Table 2). The summary of the results obtained from TG/DTA curves (temperature peaks corresponding to carbonate dissociation (T_{dis}), the total mass loss (Δm) in the temperature interval 25–1,000 °C along with the average carbonate content (G_C)) are shown in Table 2. For illustrative purposes, TG/DTA curves of selected sandstone samples are given in Figs. 12, 13, and 14 (sample 7642—free of carbonate, sample 10197—containing calcite, and sample 10577—containing dolomite, respectively).

TMA measurements

Test specimens were heated to 1,000 °C and cooled down to the room temperature. The heating rate 20 °C min^{-1} was

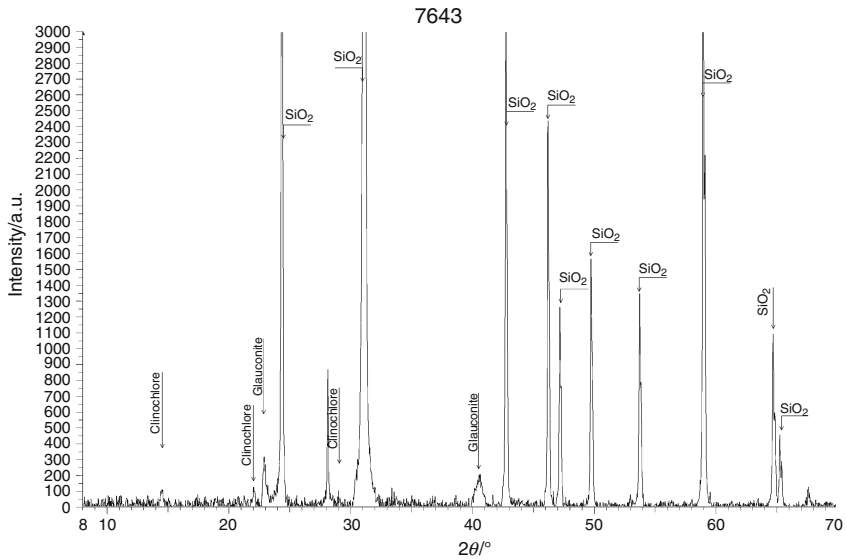

Fig. 5 XRD pattern of sample 7643

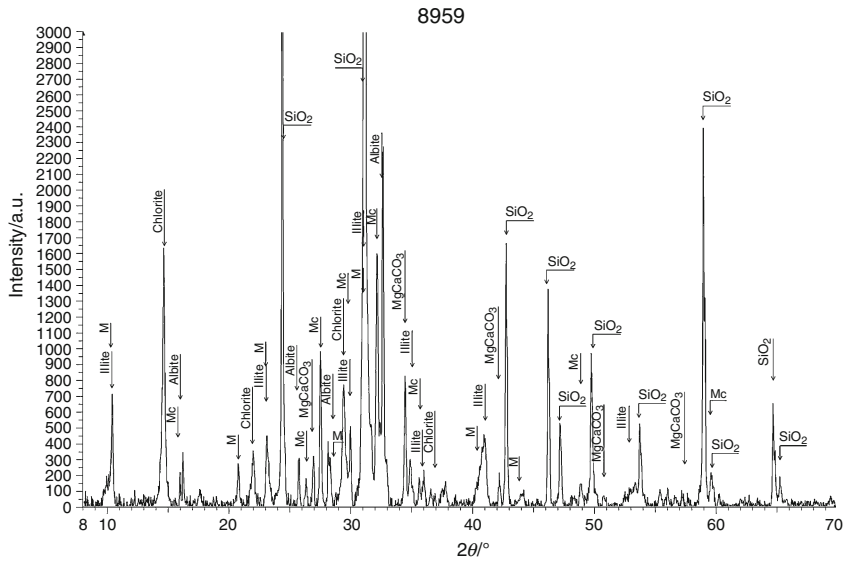

Fig. 6 XRD pattern of sample 8959

chosen because of elimination of pertinent disintegration of sandstone cubes under lower heating rates [9, 27]. Low heating rates can bring the complications with resolving thermomechanical curves. Each sandstone sample was measured in three perpendicular directions A, B, and C because of possible preferred orientation of optical axis c of quartz. The temperature, time, and deformation were recorded during heating/cooling. This procedure thus allowed us to calculate the residual thermal expansion ε (%) as a temperature normalized value [28]. Also, the changes in the length of the sample during heating (ε_H) were calculated. The coefficient of thermal expansion of the specimen was obtained by the following relationship: $\alpha \bullet l_0 = \mathrm{d}l/\mathrm{d}T$ (where α is the coefficient of thermal expansion, l_0 is the original sample length, and $\mathrm{d}l/\mathrm{d}T$ is the rate of change of sample length with temperature). Calculated values of coefficient of the linear thermal expansion α_H at the temperature range from 25 to 1,000 °C corresponded to the values of thermal expansion (ε_H) obtained from TMA curves at the same temperature interval. Percentage displacements for the tested samples are shown in Table 3.

The results of the TMA curves showed that the differences in thermal expansion during heating ε_H in directions A, B, and C for every sample were minimal. The minimal differences indicated no preference in the morphological orientation of quartz optical axis c. Therefore, it was not necessary to orient the sample and measure the expansion in three directions perpendicular to each other (coordinate system A, B, C), which is recommended e.g., for some marbles distinguished by preferred morphological orientation of calcite grains [29–31]. Also the coefficient of thermal expansion showed very similar values corresponding with minimal

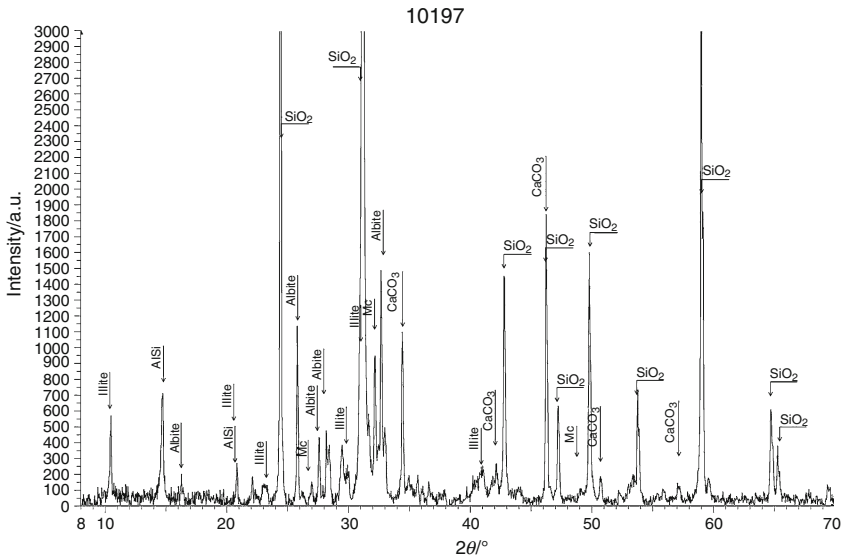

Fig. 7 XRD pattern of sample 10197

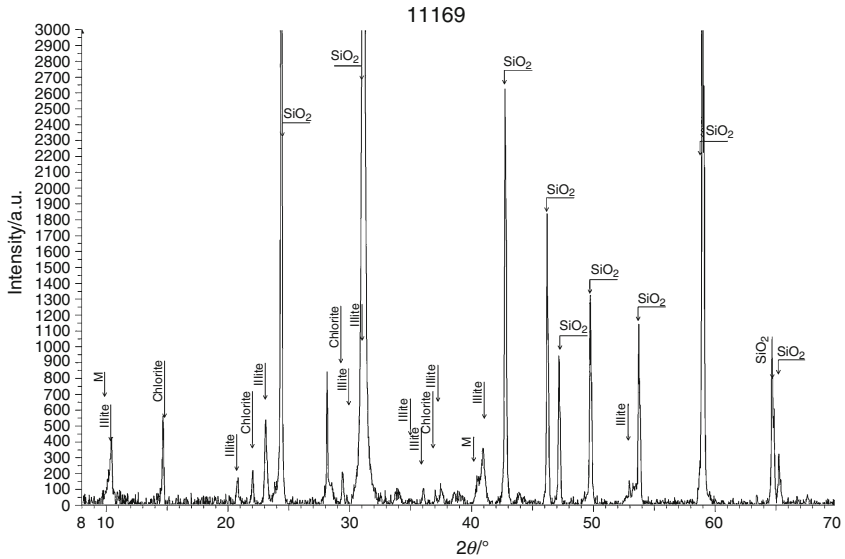

Fig. 8 XRD pattern of sample 11169

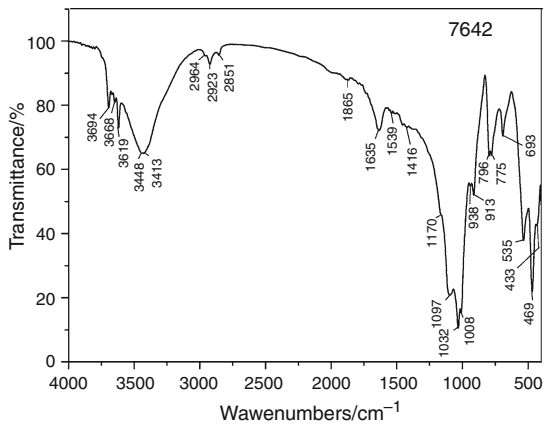

Fig. 9 FTIR spectrum of sample 7642

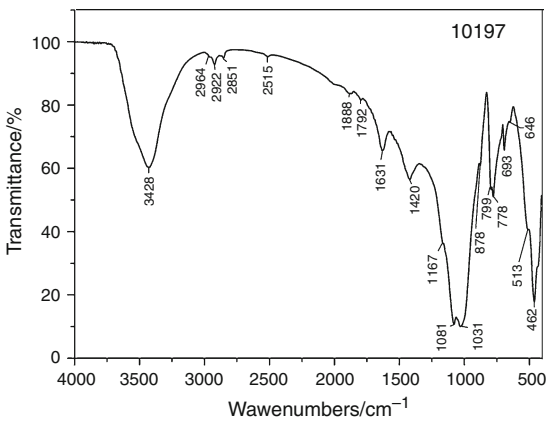

Fig. 10 FTIR spectrum of sample 10197

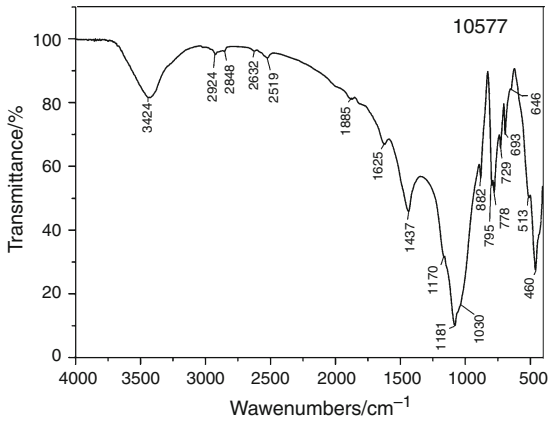

Fig. 11 FTIR spectrum of sample 10577

Table 2 Thermal data including peak temperatures of carbonate dissociation (T_{dis}), the total mass loss (Δm) and average carbonate content (G_C)

Sample	Δm/%	DTA T_{dis}/°C	G_C/%
7642	−0.5	–	–
7643	−1.5	–	–
8959	−3.2	795/819	4.0
10197	−3.1	773	10.5
10577	−6.6	810/838	18.0
10167	−2.2	767	2.0
10168	−2.5	784	2.5
10169	−2.0	–	–

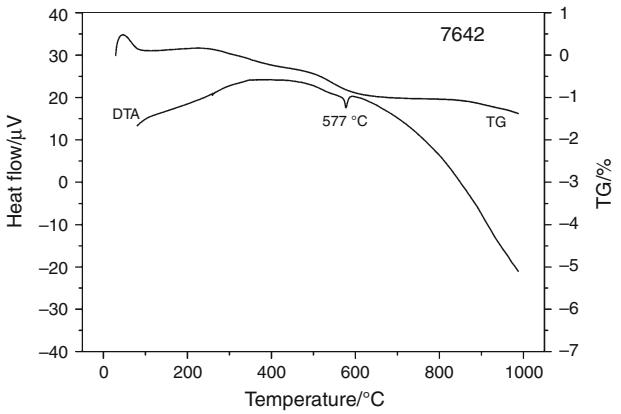

Fig. 12 TG/DTA curves of sample 7642

differences in ε_H values. It is evident, that all the tested sandstones behaved very similarly during heating, regardless of their composition and texture.

Noticeable differences were found at values of residual thermal expansion between measured samples. Values of residual thermal expansion ε ranged between 0.3 and 1%. Samples were compared in terms of their composition, texture, porosity, grain size, etc. The results showed that all

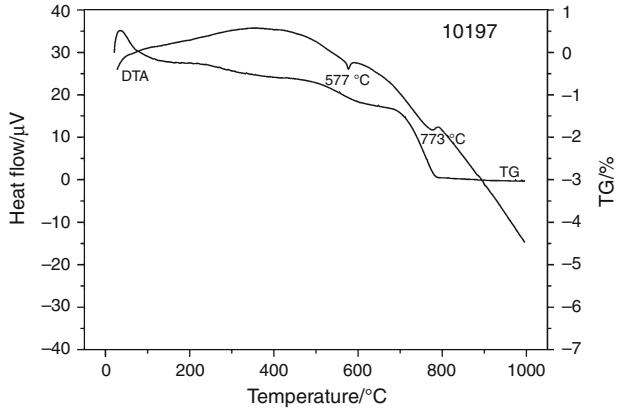

Fig. 13 TG/DTA curves of sample 10197

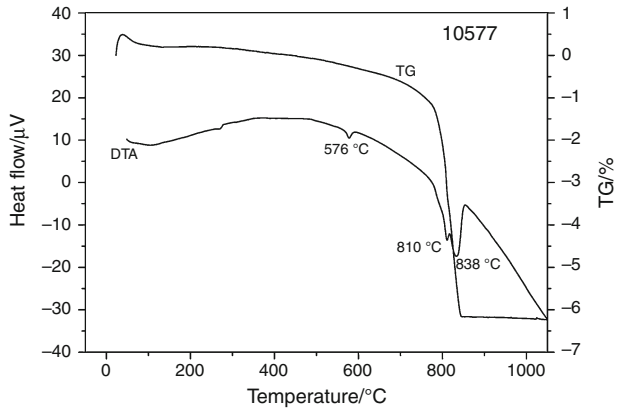

Fig. 14 TG/DTA curves of sample 10577

the seven samples can be divided into three groups according to their thermal expansion ε:

The first group involved glauconitic sandstone sample 7643 with thermal expansion ε about 0.3%. This fact is probably due to the relatively high volume of glauconite (above 20%). Gluconite has similar structure as illite and the dehydroxilation occurs at the temperature range of 550–650 °C. The removal of OH^- groups, breaking the crystal lattice and subsequent recrystallization occurs at the temperature interval 900–950 °C [25, 32]. Generated "space" may probably partially offset the increase of quartz volume because of quartz reversible modification at about 573 °C.

The second group consisted of sandstones with higher content of carbonate, and their residual thermal expansion ε was around 0.7%. In the temperature range of 750–950 °C the dissociation of carbonate and releasing of CO_2 take place. Generated "space" also did partially offset the increase of quartz volume because of reversible structural modification of quartz as in the case of glauconite dehydroxilation.

Table 3 The thermal expansion data of sandstone samples including residual thermal expansion (ε), thermal expansion during heating (ε_H) and coefficient of thermal expansion (α_H)

Sample	direction	ε/%	ε_H/%	α_H/ppm K^{-1}
7642	A	0.87	1.88	19.8
	B	0.92	1.95	20.2
	C	0.88	1.89	20.6
7643	A	0.28	1.80	19.5
	B	0.29	1.84	19.8
	C	0.33	1.88	19.4
8959	A	0.96	1.91	20.4
	B	0.97	2.00	20.0
	C	0.92	1.95	19.7
10197	A	0.73	1.95	19.8
	B	0.70	1.90	20.0
	C	0.77	1.94	20.3
10577	A	0.74	1.82	19.8
	B	0.70	1.79	20.0
	C	0.77	1.83	19.6
10167	A	0.99	1.96	19.8
	B	0.98	1.98	19.4
	C	0.96	1.95	19.3
10168	A	0.93	1.99	20.2
	B	0.95	2.02	19.7
	C	0.96	1.95	20.0
10169	A	0.87	1.88	19.8
	B	0.92	1.95	20.2
	C	0.88	1.89	20.6

The last group consists of samples with residual thermal expansion ε ranging from 0.9 to 1%. These samples (with no or minimal carbonate volume up to 10% and minimal clay mineral and mica content) contained relatively high quartz amount. The absence or minimal dehydroxilation and carbonate dissociation could not offset the quartz expansion, and therefore "the space" for compensation of quartz modification was probably insufficient. Therefore, the residual thermal expansion was higher than for other samples mentioned above. Factors such as grain size or shape of particles did not influence measured values of residual thermal expansion ε. For illustration, Figs. 15, 16, and 17 show TMA curves of selected sandstones.

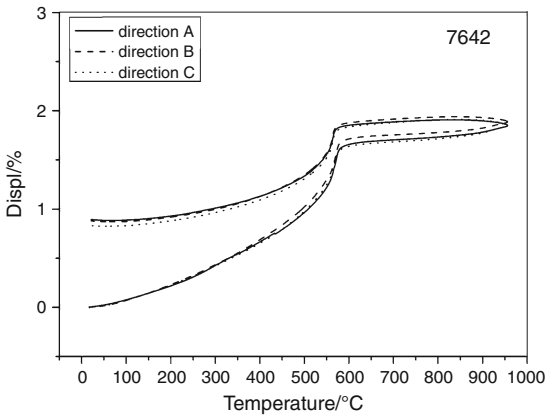

Fig. 15 TMA curve of sample 7642

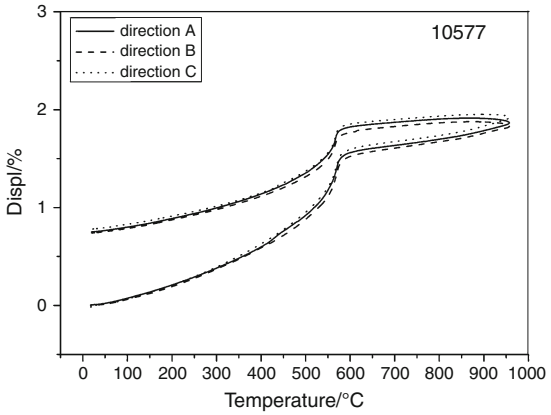

Fig. 16 TMA curve of sample 10577

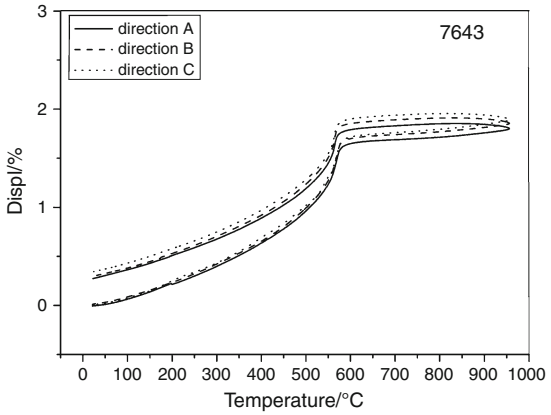

Fig. 17 TMA curve of sample 7643

Conclusions

The composition of the studied samples were similar to that of the quartz found as the main component. Small amount of illite was found in all the studied samples. Other components like mica, muscovite, biotite, feldspar, chlorite, and kaolinite were found only in a few samples. One sample contained a significant amount of glauconite, and the presence of carbonate (calcite, dolomite, or siderite) was found in five samples. Samples were identified by microscopic analysis as grainy with porous structure, from medium to poor sorting, with only sandstone samples 7643 and 11167 being classified as a good sorting. Thermal expansion in directions A, B, and C for each sample was almost identical. The minimal differences indicated no

preferred morphological orientation of quartz grains along with no prior orientation of quartz optical axis c. The thermal expansion coefficient of heating (α_H) as well as the thermal expansion during heating ε_H demonstrated similar values. Coefficient α_H was around 20 ppm K^{-1} and values of thermal expansion ε_H varied from 1.8 to 2.0%. In the case of residual thermal expansion ε, some differences between samples have been already found. The maximum values of residual thermal expansion ε were detected in samples with higher content of quartz and rock fragments and with relatively low content of clay minerals and carbonate content of up to 10%. Middle values were found for samples with higher content of carbonate (more than 10%) and lower content of quartz. The lowest value of residual thermal expansion ε was detected for the sample with relatively high content of glauconite (above 20%). It is evident that mainly the amount of quartz and the higher volume of clay minerals, glauconite, and carbonates play the main role in resultant sandstone residual thermal expansion. The other factors such as grain size or shape of particles did not significantly influence the observed values of residual thermal expansion ε.

Acknowledgements This study was supported by the Czech Science Foundation, the projects: No. 105/08/1398, No. 105/09/P397, No. 105/07/P416, and by the Research plan No. AVOZ 30860518. The authors would like to thank George Laynr for controlling and correcting the use of English in this article.

References

1. Procházka J. Kvalitativní charakteristika cenomanských pískovců hořického hřbetu (Qualitative characteristics of the Cenomanian sandstones of the Horice bridge). Geochemie. 1986;21:200–32 (in Czech with English summary).
2. Pospíšil P. Cretaceous sandstones in Moravia and Silesia and their application as building and ornamental stones. Bull Geosci. 2004;79(3):183–93.
3. Rawlley RK. Mineralogical investigations on an Indian glauconitic sandstone of Madhya Pradesh state. Appl Clay Sci. 1994;8:449–65.
4. Andreozzi M, et al. Geochemical and mineralogical criteria for the identification of ash layers in the stratigraphic framework of a foredeep; the Early Miocene Mt. Cervarola Sandstones, northern Italy. Chem Geol. 1997;137:23–39.
5. Kiminami K, Fujii K. The relationship between major element concentration and grain size within sandstones from four turbidite sequences in Japan. Sediment Geol. 2007;195:203–15.
6. Khidir A, Catuneanu O. Reservoir characterization of Scollard-age fluvial sandstones, Alberta foredeep. Mar Pet Geol. 2010. doi:10.1016/j.marpetgeo.2010.05.001.
7. Ip KH, Stuart BH, Thomas PS, Ray AS. Thermal characterization of the clay binder of heritage Sydney sandstones. J Therm Anal Calorim. 2008;92:97–100.
8. Yas E, et al. Determination of the thermal conductivity from physico-mechanical properties. Bull Eng Geol Environ. 2008;67:219–25.
9. Martinec P, Vavro M, Ščučka J, Mašláň M. Properties and durability assessment of glauconitic sandstone: a case study on Zamel sandstone from the Bohemian Cretaceous Basin (Czech Republic). Eng Geol. 2009. doi:10.1016/j.enggeo.2009.08.005.
10. Jeng FS, et al. Influence of petrographic parameters on geotechnical properties of tertiary sandstones from Taiwan. Eng Geol. 2004;73:71–91.
11. Baud P, Klein E, Wong T. Compaction localization in porous sandstones: spatial evolution of damage and acoustic emission activity. J Struct Geol. 2004;26:603–24.
12. Bésuelle P. Compacting and dilating shear bands in porous rocks: theoretical and experimental conditions. J Geophys Res. 2001;106:1335–42.
13. El Bied A, Sulem J, Martineau F. Microstructure of shear zones in Fontainebleau sandstone. Int J Rock Mech Min Sci. 2002;39:917–32.
14. Said S, et al. Use of X-ray powder diffraction for quantitative analysis of carbonate rock reservoir samples. Powder Technol. 2007;175:115–21.
15. Blanc F, et al. Estimate of clay minerals amounts from XRD pattern modeling. Phys Chem Earth. 2007;32:135–44.
16. Chmielová M, Weiss Z. Determination of structural disorder degree using an XRD profile fitting procedure. Application to Czech kaolins. Appl Clay Sci. 2002;22:65–74.
17. Farmer VC. The infrared spectra of minerals. London: Mineralogical Society; 1974.
18. Madejová J, Komadel P. Baseline studies of the clay minerals society source clays: infrared methods. Clays Clay Miner. 2001;49(5):410–32.
19. Krivácsy Z, Hlavay J. Determination of quartz in dust samples by diffuse reflection FTIR spectroscopy. J Mol Struct. 1993;294:251–4.
20. Oinuma K, Hayashi H. Infrared study of mixed-layer clay minerals. Am Mineral. 1965;50:1213–27.
21. Vaculíková L, Plevová E. The identification of clay minerals and micas in sedimentary rocks. Acta Geodyn Geomater. 2005;2(2):163–71.
22. Fuente S, Cuadros J, Linares J. Early stages of volcanic tuff alteration in hydrothermal experiments: formation of mixed-layer illite-smectite. Clays Clay Miner. 2002;50:578–90.
23. Hatakeyama T, Liu Z. Handbook of thermal analysis. New York: Wiley; 1998.
24. Blažek A. Book of thermal analysis. Prague: SNTL; 1974.
25. Muller F, Drits V, Plancon A, Robert JL. Structural transformation of 2:1 dioctahedral layer silicates during dehydroxylation–rehydroxylation reactions. Clays Clay Miner. 2000;48:572–85.
26. Smykatz-Kloss W, Klinke W. The determination of authigenic quartz in porous sedimentary rocks by means of differential scanning calorimetry. J Therm Anal Calorim. 1994;42:85–97.
27. Plevová E, Kožušníková A, Vaculíková L, Simha Martynková G. Thermal behavior of selected Czech marble samples. J Therm Anal Calorim. 2010. doi:10.1007/s10973-010-0907-5.
28. Price DM. Principles of thermal analysis and calorimetry. Cambridge: The Royal Society of Chemistry; 1994.
29. Obara B, Kožušníková A. Utilisation of the image analysis method for the detection of the morphological anisotropy of calcite grains in marble. Comput Geosci. 2007;11(4):275–81.
30. Leiss B, Weiss T. Fabric anisotropy and its influence on physical weathering of different types of Carrara marbles. J Struct Geol. 2000;22:1737–45.
31. Luque A, et al. Anisotropic behaviour of White Macael marble used in the Alhambra of Granada (Spain). The role of thermo-hydric expansion in stone durability. Eng Geol. 2009. doi:10.1016/j.enggeo.2009.06.015.
32. Thompson GR, Hower J. The mineralogy of glauconite. Clays Clay Miner. 1975;23:289–300.